NEUROSCIENCE

Bright and photostable chemigenetic indicators for extended in vivo voltage imaging

Ahmed S. Abdelfattah[1]*, Takashi Kawashima[1]*†, Amrita Singh[1,2], Ondrej Novak[1,3], Hui Liu[1], Yichun Shuai[1], Yi-Chieh Huang[4], Luke Campagnola[5], Stephanie C. Seeman[5], Jianing Yu[1], Jihong Zheng[1], Jonathan B. Grimm[1], Ronak Patel[1], Johannes Friedrich[6,7,8], Brett D. Mensh[1], Liam Paninski[6,7], John J. Macklin[1], Gabe J. Murphy[5], Kaspar Podgorski[1], Bei-Jung Lin[4], Tsai-Wen Chen[4], Glenn C. Turner[1], Zhe Liu[1], Minoru Koyama[1], Karel Svoboda[1], Misha B. Ahrens[1]‡, Luke D. Lavis[1]‡, Eric R. Schreiter[1]‡§

Genetically encoded voltage indicators (GEVIs) enable monitoring of neuronal activity at high spatial and temporal resolution. However, the utility of existing GEVIs has been limited by the brightness and photostability of fluorescent proteins and rhodopsins. We engineered a GEVI, called Voltron, that uses bright and photostable synthetic dyes instead of protein-based fluorophores, thereby extending the number of neurons imaged simultaneously in vivo by a factor of 10 and enabling imaging for significantly longer durations relative to existing GEVIs. We used Voltron for in vivo voltage imaging in mice, zebrafish, and fruit flies. In the mouse cortex, Voltron allowed single-trial recording of spikes and subthreshold voltage signals from dozens of neurons simultaneously over a 15-minute period of continuous imaging. In larval zebrafish, Voltron enabled the precise correlation of spike timing with behavior.

Animal behavior is produced by patterns of neuronal activity that span a wide range of spatial and temporal scales. Understanding how neural circuits mediate behavior thus requires high-speed recording from ensembles of neurons for long periods of time. Although the activity of large numbers of neurons can now be routinely recorded using genetically encoded calcium indicators (GECIs) (*1*), the slow kinetics of calcium signals complicate the measurement of action potentials, and subthreshold voltage signals are missed entirely (*1*–*3*). Voltage imaging using genetically encoded voltage indicators (GEVIs) can overcome these challenges, enabling imaging of fast spikes and subthreshold dynamics in genetically defined neurons (*4*, *5*). The high imaging speed and excitation intensity required for voltage imaging, combined with the smaller volume of the cellular membrane, place increased demands on voltage indicators relative to GECIs. Extant GEVIs rely on fluorescence from either microbial rhodopsins (*6*–*8*) or fluorescent proteins (*9*–*13*). These fluorophores lack the brightness and photostability to allow in vivo voltage imaging from large fields of view over time scales of many behavioral events, precluding the millisecond–time scale analysis of neural circuits. Improved rhodamine dyes such as the Janelia Fluor (JF) dyes can be used in complex biological experiments because of their high brightness and photostability (*14*), compatibility with self-labeling protein tags (*15*, *16*), and ability to traverse the blood-brain barrier for in vivo delivery (*17*). We describe a "chemigenetic," or hybrid protein–small molecule, GEVI scaffold that we call Voltron, which irreversibly binds these synthetic fluorophore dyes. Voltron provides an increased photon yield that enables in vivo imaging of neuronal spiking and subthreshold voltage signals in model organisms with order-of-magnitude improvement in the number of neurons imaged simultaneously over substantially longer durations.

Our design for a chemigenetic voltage indicator combines a voltage-sensitive microbial rhodopsin domain (*6*, *7*, *11*) with a dye-capture protein domain (Fig. 1A) that irreversibly binds a synthetic fluorophore dye ligand (*14*, *15*) (Fig. 1B), analogous to previously reported voltage indicators that use fluorescent proteins (*10*, *11*, *18*). Transmembrane voltage–dependent changes in the absorption spectrum (*6*, *19*) of the rhodopsin domain of Voltron reversibly modulate the degree of fluorescence quenching of the nearby bound dye through Förster resonance energy transfer (FRET). We investigated the modularity of this approach, finding that three different rhodopsin domains—QuasAr1 (*7*), QuasAr2 (*7*), and Ace2N (*11*, *20*)—modulated the fluorescence of the rhodamine dye Janelia Fluor 549 (JF_{549}) after binding to either HaloTag (*15*) or SNAP-tag (*21*) dye-capture protein domains (figs. S1 to S8). Removing a small number of amino acid residues at the junction of the rhodopsin and self-labeling tag domains increased the amplitude of fluorescent voltage signals (fig. S1), presumably by decreasing average distance and thus increasing FRET efficiency between the dye and rhodopsin retinal cofactor. The configuration providing the best signal-to-noise ratio (SNR) for spikes was Ace2N fused to HaloTag with five amino acids removed at their junction (Fig. 1, A and B, and fig. S2), hereafter referred to as Voltron.

We tested several Voltron-dye combinations in cultured rat neurons and acute mouse brain slices with high-speed imaging and simultaneous whole-cell patch clamp electrophysiology (Fig. 1C, figs. S6 and S9 to S13, and tables S1 and S2). Voltron could detect neuronal action potentials and subthreshold potential changes with a variety of JF dye ligands with emission maxima between 520 nm and 660 nm using fluorescence imaging with one-photon excitation (Fig. 1, C to E, and fig. S6) but was not compatible with two-photon imaging, as described previously for rhodopsin-containing GEVIs (*22*, *23*). Voltron bound to JF_{525} ($Voltron_{525}$) exhibited the highest sensitivity, giving a fluorescence change of −23 ± 1% $\Delta F/F_0$ for a voltage step from −70 mV to +30 mV (Fig. 1E and fig. S9); $Voltron_{549}$ showed similar sensitivity. $Voltron_{525}$ responded to voltage steps with submillisecond on and off time constants (table S3 and fig. S10). We compared the brightness and photostability of Voltron in neuronal cultures with those of two other fluorescent protein–based GEVIs: Ace2N-mNeon (*11*) and ASAP2f (*13*). Both $Voltron_{525}$ and $Voltron_{549}$ were brighter than Ace2N-mNeon (by a factor of 3 to 4) and ASAP2f (by a factor of 16 to 18) (Fig. 1F) in cell culture. This difference did not result from differences in expression; we compared the brightness of $Voltron_{549}$ and Ace2N-mNeon at the single-molecule level and observed a similar brightness difference (factor of 3 to 4) (Fig. 1G). $Voltron_{525}$ and $Voltron_{549}$ were also more photostable in ensemble measurements (Fig. 1H, tables S4 and S5, and figs. S14 and S15) as well as in single-molecule assays, in which photobleaching times were longer for $Voltron_{549}$ than those of Ace2N-mNeon by a factor of 8 (Fig. 1I). Overall, the improved brightness and photostability of Voltron increased the photon yield by at least a factor of 10 in neurons relative to existing GEVIs that rely on fluorescent proteins.

In vivo, Voltron could be reliably expressed and labeled with dye in mice, larval zebrafish, and adult fruit flies (Figs. 1 to 4 and figs. S16 to S19 and S21 to S45). Simultaneous in vivo electrophysiology and Voltron imaging in each of these organisms confirmed the detection of individual action potentials (Fig. 1, J and K, and figs. S17 to S19). For imaging in the mouse brain,

[1]Janelia Research Campus, Howard Hughes Medical Institute, Ashburn, VA 20147, USA. [2]Solomon H. Snyder Department of Neuroscience, Johns Hopkins University, Baltimore, MD 21205, USA. [3]Department of Auditory Neuroscience, Institute of Experimental Medicine, Academy of Sciences of the Czech Republic, Prague, Czech Republic. [4]Institute of Neuroscience, National Yang-Ming University, Taipei 112, Taiwan. [5]Allen Institute for Brain Science, Seattle, WA 98109, USA. [6]Department of Statistics and Center for Theoretical Neuroscience, Columbia University, New York, NY 10027, USA. [7]Department of Neuroscience and Grossman Center for the Statistics of Mind, Columbia University, New York, NY 10027, USA. [8]Center for Computational Biology, Flatiron Institute, New York, NY 10010, USA.
*These authors contributed equally to this work. †Present address: Department of Neurobiology, Weizmann Institute of Science, Rehovot, Israel. ‡These authors contributed equally to this work. §Corresponding author. Email: schreitere@janelia.hhmi.org

we used a variant of Voltron appended with a 63–amino acid sequence from the rat potassium channel Kv2.1 that restricts expression to the membrane of the cell body and proximal dendrites (*24*, *25*) (Voltron-ST; fig. S20). The rapid kinetics of Voltron$_{525}$-ST allowed clear observation of action potentials in fast-spiking parvalbumin (PV)–expressing interneurons in the CA1 region of the mouse hippocampus (Fig. 2, A to G, and fig. S21). We measured the orientation tuning of the spiking and subthreshold responses of cortical layer 2/3 pyramidal neurons in mouse primary visual cortex in response to the mouse observing directional movement of light and dark stripes, a benchmark for new indicators (*1*, *11*) (Fig. 2, H to L, and figs. S22 to S24), and confirmed that spiking activity showed sharper orientation selectivity than did subthreshold voltage signals

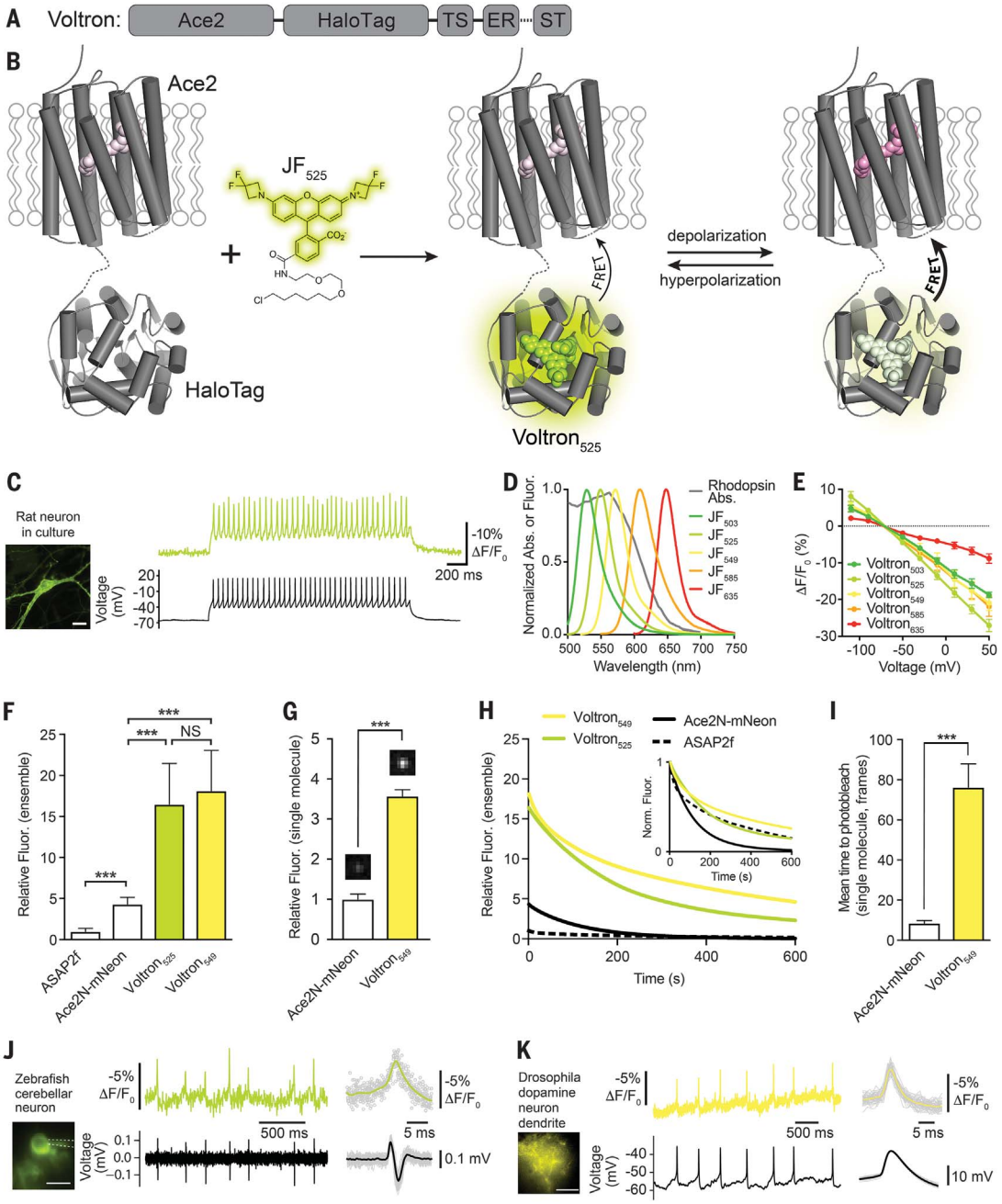

Fig. 1. Development of the chemigenetic voltage indicator Voltron. (**A**) Schematic of Voltron sequence: A rhodopsin (Ace2) is fused to a self-labeling tag domain (HaloTag) with additional sequences added to improve or localize membrane targeting: Golgi export trafficking sequence (TS), endoplasmic reticulum export sequence (ER), and somatic targeting sequence (ST). (**B**) Model of Voltron mechanism. (**C**) Left: Cultured rat hippocampal neuron expressing Voltron and labeled with JF$_{525}$. Scale bar, 20 μm. Right: Single-trial recording of action potentials and subthreshold voltage signals from current injections in primary neuron culture using 400-Hz imaging (top, fluorescence) or electrophysiology (bottom, membrane potential). (**D**) Fluorescence emission spectra of different JF dyes overlaid with the absorbance spectrum of Ace2N. (**E**) Fluorescence change as a function of membrane voltage with different JF dye–Voltron conjugates. (**F**) Relative fluorescence of ASAP2f, Ace2N-mNeon, Voltron$_{525}$, and Voltron$_{549}$ in cultured neurons (n = 70, 68, 48, and 62 measurements, respectively, from five independent transfections for each construct). Illumination intensity was ~10 mW/mm^2 at imaging plane. ***P < 0.001 [one-way analysis of variance (ANOVA) followed by Bonferroni test on each pair]; NS, not significant. Fluorescence was normalized to ASAP2f mean intensity. (**G**) Relative single-molecule brightness of Ace2N-mNeon and Voltron$_{549}$. ***P < 0.001 (two-tailed Student t test). (**H**) Bleaching curves for ASAP2f, Ace2N-mNeon, Voltron$_{525}$, and Voltron$_{549}$ in primary neuron culture. Illumination intensity was ~23 mW/mm^2 at imaging plane. Bleaching curves were normalized to mean cellular fluorescence from (F) or normalized to the zero-time value (inset). (**I**) Mean time to bleach of Ace2N-mNeon and Voltron$_{549}$ during single-molecule imaging, 100-ms frames. ***P < 0.001 (two-tailed Student t test). (**J** and **K**) Simultaneous in vivo Voltron imaging (300 and 800 Hz, top) and electrophysiology (bottom) in larval zebrafish (extracellular) and adult *Drosophila* (whole-cell), respectively. Spike-triggered averages are shown at the right. Scale bars, 20 μm.

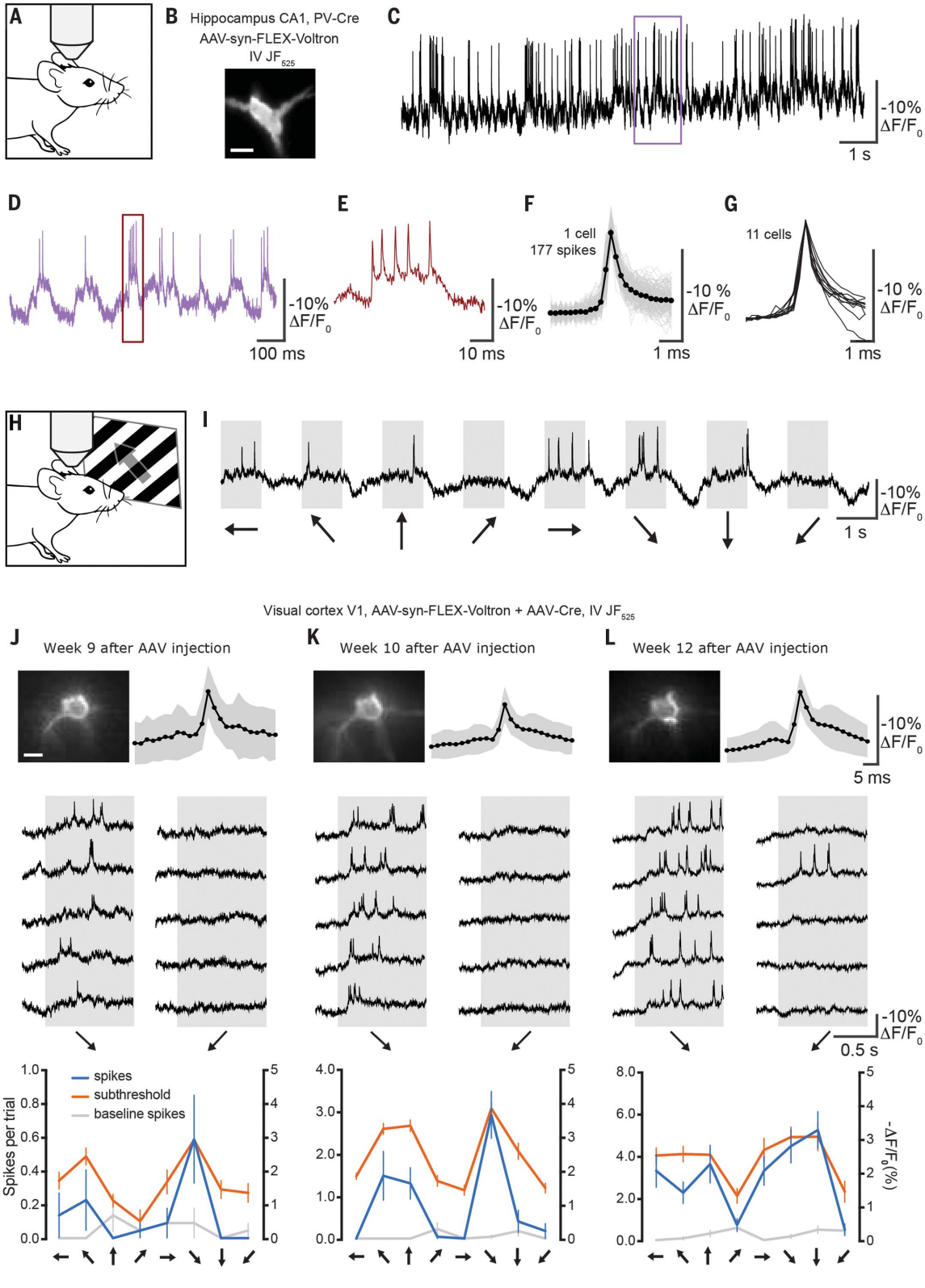

Fig. 2. Using Voltron to measure membrane voltage dynamics in hippocampal PV neurons and visual cortex pyramidal neurons of mice. (**A**) Schematic of imaging of spontaneous activity in the CA1 region of the hippocampus of an awake mouse. (**B**) Image of hippocampal PV neuron expressing Voltron labeled with JF_{525}. Scale bar, 20 μm. (**C** to **E**) $Voltron_{525}$ raw $\Delta F/F_0$ traces showing spontaneous spikes of a PV neuron (B) located at a depth of 60 μm in the hippocampal CA1 region of a fully awake mouse imaged at 3858 frames per second. Color-coded boxes indicate regions shown at expanded time scales. (D) is a zoom of the boxed region from (C); (E) is a zoom of the boxed region from (D). (**F**) Overlay of 177 spikes detected during a 15-s period (gray) and their average (black). (**G**) Spike shape of 11 PV neurons. (**H**) Schematic of imaging of primary visual cortex of an anesthetized mouse during display of drifting grating visual stimuli. (**I**) Example trace showing 500-Hz Voltron fluorescence during one trial of a sequence of visual stimuli. Arrows below represent the direction of movement of the drifting grating. (**J** to **L**) Top left: Images of a pyramidal cell at a depth of 148 μm, imaged three times over a period of 4 weeks at the indicated number of weeks after virus injection. Scale bar, 10 μm. Top right: Average of all spikes in session (black) and SD (gray). Middle: Raw $\Delta F/F_0$ trace for five repetitions in each session, showing two orthogonal orientations (indicated with arrows below) from the neuron pictured at top left. Bottom: Orientation tuning to full-frame drifting gratings of the neuron pictured at top left, displayed as number of spikes during trials (blue), number of spikes during preceding intertrial intervals (gray), and subthreshold $\Delta F/F_0$ (right *y* axis) after low-pass filtering traces using a 10-point median filter. For each orientation, subthreshold response is calculated by averaging the low-pass–filtered trace between 100 and 400 ms after trial onset, and baseline is calculated by averaging the low-pass–filtered trace from 80 ms preceding trial onset to 20 ms after trial onset. Data are displayed as response minus baseline. Error bars represent SEM (20 to 22 repetitions per session).

(*26*). We extended the imaging period over several consecutive weeks by injecting additional JF_{525} HaloTag ligand before each imaging session (Fig. 2, J to L, and fig. S24).

Next, we attempted to image larger areas containing more neurons for longer times in vivo in mouse cortex (Fig. 3). By wide-field microscopy at illumination intensities between 3 and 20 mW/mm^2, we could clearly identify and distinguish action potentials from nearby neurons throughout 15 min of continuous imaging (SNR = 5.3 during the first minute, 4.4 during the final minute) (Fig. 3, B to E). We expanded the field of view to include dozens of cortical interneurons labeled with $Voltron_{525}$-ST in a transgenic mouse line (NDNF-Cre) (*27*) while imaging at 400 Hz (Fig. 3, F and G, and figs. S25 to S42). Overall, we imaged a total of 449 neurons (12 fields of view in three mice), demonstrating routine voltage imaging of populations of neurons in superficial mouse cortex (Fig. 3G and figs. S25 to S42). This scale of in vivo voltage imaging enabled analysis of membrane potential correlations between many neuron pairs (fig. S26).

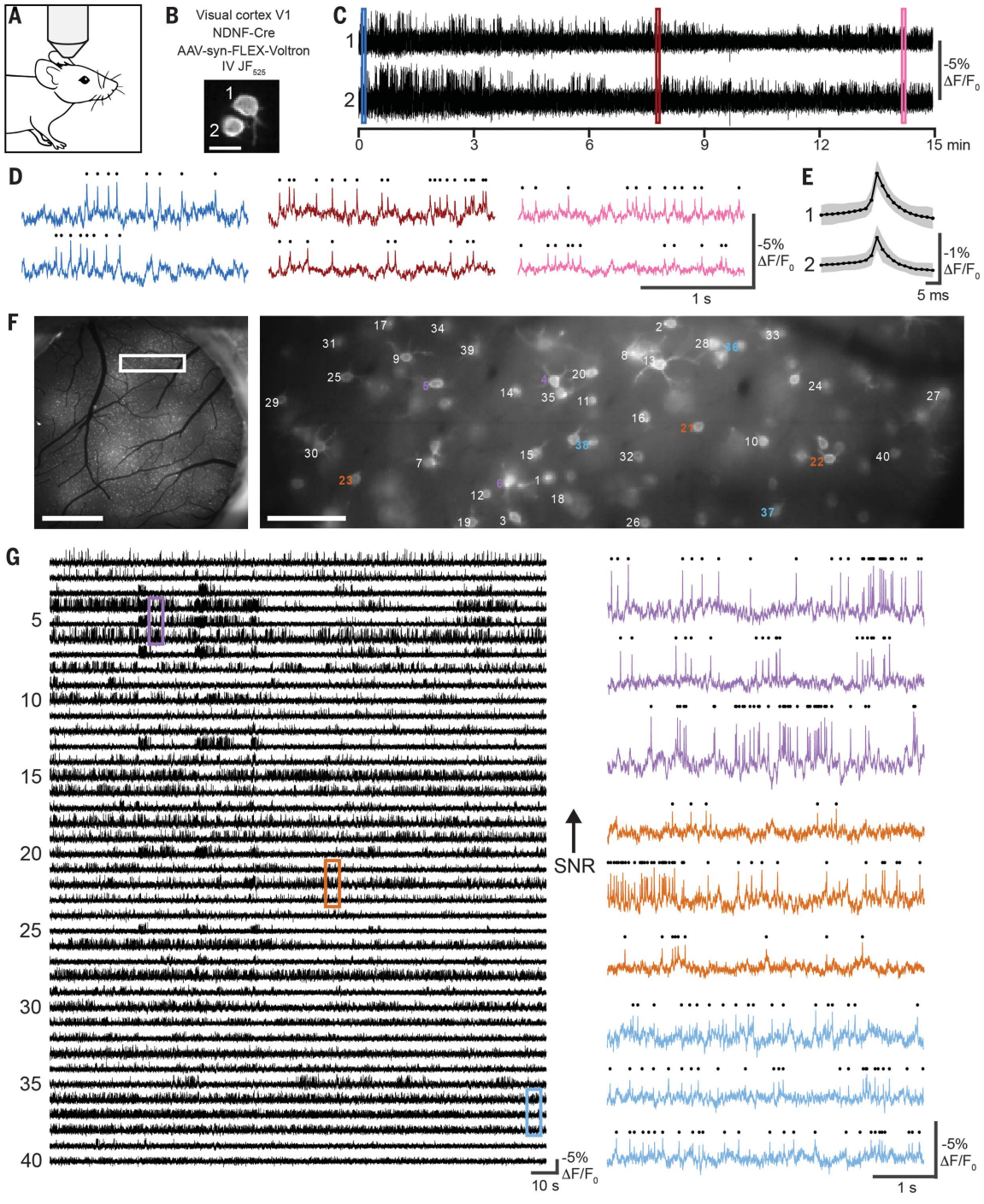

Fig. 3. Imaging of voltage activity in large fields of view of the mouse neocortex over long durations. (**A**) Schematic of the imaging setup. (**B**) Image of two neurons expressing $Voltron_{525}$-ST in layer 1 of the visual cortex of an NDNF-Cre mouse. Scale bar, 10 μm. (**C**) $\Delta F/F_0$ traces from neurons in (B), recorded over 15 min at 400 Hz. (**D**) Color-coded zooms of indicated regions of the traces in (C), with detected action potentials indicated by black dots above the fluorescence traces. (**E**) Average of all spikes in session (black) and SD (gray). (**F**) Left: Fluorescence image of a cranial window over primary visual cortex (V1) in an NDNF-Cre mouse showing Cre-dependent expression of $Voltron_{525}$-ST (bright spots). Scale bar, 1 mm. Right: Zoomed image of left panel in the area indicated by the white rectangle, with neuron labels corresponding to fluorescence traces in (G). Scale bar, 100 μm. (**G**) Left: $\Delta F/F_0$ traces during 3 min of recording at 400 Hz from neurons pictured in (F), in decreasing order of SNR. Right: Zooms of $\Delta F/F_0$ traces from color-coded regions of (G) with detected action potentials represented as black dots above, illustrating representative traces with high (top), medium (middle), and low (bottom) SNR. Traces have been background-subtracted, which removes shared subthreshold membrane potential fluctuations (compare to fig. S25 without subtraction).

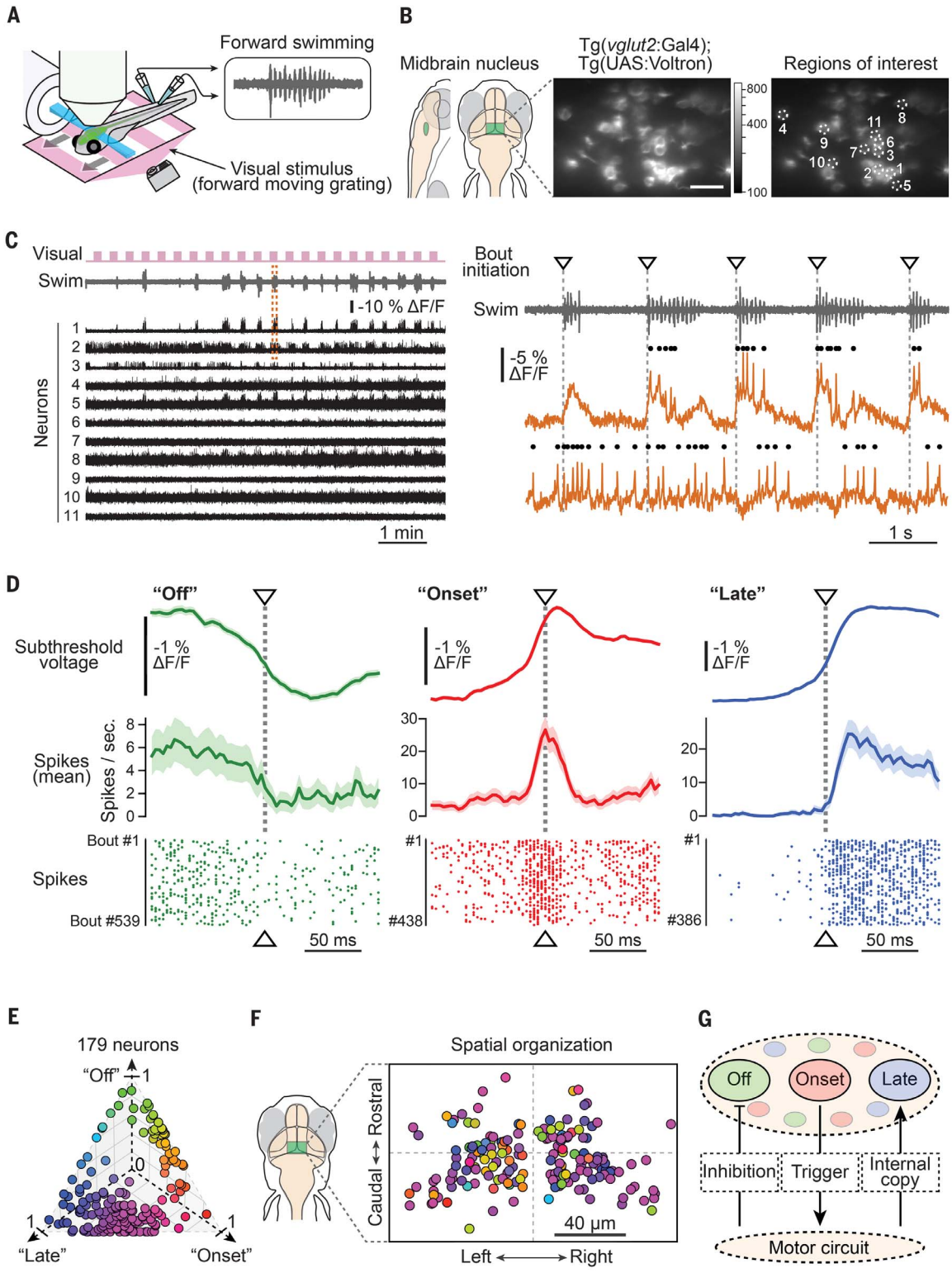

Fig. 4. Voltron reveals millisecond–time scale neural dynamics during swimming behavior in zebrafish. (**A**) Schematic illustration of the setup. An immobilized zebrafish is placed under the light-sheet microscope, and the motor signals (inset) from its tail are recorded using a pair of electrodes. Visual stimuli (forward-drifting gratings) for eliciting swimming responses are presented below the fish. (**B**) Left: Anatomical location of the imaged brain region (midbrain nucleus; see fig. S44A). Center: Representative field of view of the imaged region expressing Voltron. Scale bar, 20 μm. Right: Position of neurons analyzed in (C). (**C**) Left: Periods of visual motion (pink) and swim signals (gray) are plotted above Voltron fluorescence traces (black) simultaneously recorded from 11 neurons shown in (B). Right: Zoom of swimming signals (top) and Voltron fluorescence traces from two representative neurons (bottom) are expanded from the dashed box in the left panel. Dots at the top of each trace represent action potentials recognized by the algorithm described in fig. S45, A and B. Inverted triangles and dotted gray lines indicate initiation of each swim bout. (**D**) Mean subthreshold signal (top), mean frequency of action potentials (middle), and raster plots of action potentials (bottom) near the initiation of swim bouts from three representative neurons: "Off" (green), "Onset" (red), and "Late" (blue). Shadows in the top and middle panels represent SEM across swim events. (**E**) Classification of recorded neurons by their mean subthreshold signals near the initiation of swim bouts; 179 neurons recorded from 43 fish were classified using non-negative matrix factorization and colored according to the weights for three factors: "Onset" (red), "Off" (green), and "Late" (blue). See supplementary materials for details of this classification. (**F**) Spatial organization of the same population of neurons as in (E). Neurons from multiple fish are superimposed on a single map according to the distance from the center of this midbrain nucleus. (**G**) Hypothetical model of neural activity modulation in this midbrain nucleus.

We used Voltron to image zebrafish larvae, which respond to visual input with fast, directed swim bouts that are tailored to the details of the stimulus (*28*). We sought to uncover how this sensory-to-motor transformation unfolds in neuronal populations at fine time scales that are inaccessible with calcium imaging. We verified that Voltron could detect action potentials and subthreshold voltage signals in live zebrafish after labeling with several different colors of dye ligands (figs. S17 and S43). We then used Voltron$_{525}$ to monitor neural activity during swim bouts induced by visual motion (Fig. 4A). We recorded Voltron signals from 179 neurons across 43 fish in a motor-sensory nucleus in the tegmental area of the midbrain (Fig. 4B and fig. S44), yielding data on subthreshold membrane voltage modulation as well as automatically detected spike times (Fig. 4C and fig. S45). We found neuron populations with different temporal activity patterns, including neurons whose firing rate increased ~1 s before the fish started swimming (fig. S44, B and C, "Ramp"), neurons whose firing rate was suppressed each time the fish swam (Fig. 4D, "Off"), and neurons that fired each time the fish swam (Fig. 4D, "Onset" and "Late"). Of the latter types, some fired just before swimming (~20 ms before swim onset, "Onset") and others fired just after swimming (~10 ms after swim onset, "Late"). There was a change in subthreshold voltage that preceded these firing rate changes by tens of milliseconds (Fig. 4D and fig. S44D). The neuron types were spatially intermingled within this midbrain nucleus (Fig. 4, E and F). The existence of neurons that fired before swimming and neurons that fired after swimming may indicate that this nucleus both partakes in the generation of swim bouts and is influenced by the motor output (Fig. 4G). Thus, Voltron allows for the dissection of population motor coding and sensorimotor integration circuits in ways that neither single-cell electrophysiology nor population calcium imaging can.

We tested Voltron in adult *Drosophila* in vivo by expressing the protein in a pair of dopaminergic neurons, one in each brain hemisphere, which innervate a single compartment in the mushroom body. We detected strong spiking signals from axons and dendrites of these neurons with Voltron$_{549}$ (Fig. 1K and fig. S18). The fluorescence signals matched action potentials detected using electrophysiology. In some neuronal cell types in *Drosophila*, calcium indicators located in the cell body have failed to exhibit fluorescence changes even under conditions where high spike rates are expected (*29*). However, spikes were clearly detectable when imaging from the soma of dopamine neurons with Voltron (fig. S18E). We could clearly distinguish spikes from the two neurons according to the amplitude of the spiking signals even when imaging from neuropil where their axons overlap extensively, likely because each bilaterally projecting cell contributes a denser innervation of the mushroom body in the ipsilateral hemisphere (fig. S18D).

Combining the molecular specificity of genetically encoded reagents with the superior photophysics of chemical dyes is an established path to improved imaging reagents (*14*). However, previous attempts to create hybrid protein–small molecule indicators by various approaches have not been successful for in vivo imaging (*30*). We engineered a modular sensor scaffold in which the targeting and sensor domains are genetically encoded and only the fluorophore and its protein-binding anchor are synthetic. The resulting chemigenetic indicator, Voltron, exhibits increased photon output, enabling in vivo voltage imaging of many more neurons over longer times—approximately 10^2 more neuron-minutes than other sensors. This improvement enables imaging experiments that can help to reveal how the precise electrical dynamics of neuronal populations orchestrate behavior over different time scales.

REFERENCES AND NOTES

1. T. W. Chen *et al*., *Nature* **499**, 295–300 (2013).
2. K. Svoboda, W. Denk, D. Kleinfeld, D. W. Tank, *Nature* **385**, 161–165 (1997).
3. V. Emiliani, A. E. Cohen, K. Deisseroth, M. Häusser, *J. Neurosci.* **35**, 13917–13926 (2015).
4. Y. Xu, P. Zou, A. E. Cohen, *Curr. Opin. Chem. Biol.* **39**, 1–10 (2017).
5. M. Z. Lin, M. J. Schnitzer, *Nat. Neurosci.* **19**, 1142–1153 (2016).
6. J. M. Kralj, A. D. Douglass, D. R. Hochbaum, D. Maclaurin, A. E. Cohen, *Nat. Methods* **9**, 90–95 (2011).
7. D. R. Hochbaum *et al*., *Nat. Methods* **11**, 825–833 (2014).
8. Y. Adam *et al*., *Nature* **569**, 413–417 (2019).
9. L. Jin *et al*., *Neuron* **75**, 779–785 (2012).
10. P. Zou *et al*., *Nat. Commun.* **5**, 4625 (2014).
11. Y. Gong *et al*., *Science* **350**, 1361–1366 (2015).
12. A. S. Abdelfattah *et al*., *J. Neurosci.* **36**, 2458–2472 (2016).
13. H. H. H. Yang *et al*., *Cell* **166**, 245–257 (2016).
14. J. B. Grimm *et al*., *Nat. Methods* **12**, 244–250 (2015).
15. G. V. Los *et al*., *ACS Chem. Biol.* **3**, 373–382 (2008).
16. L. P. Encell *et al*., *Curr. Chem. Genomics* **6**, 55–71 (2012).
17. J. B. Grimm *et al*., *Nat. Methods* **14**, 987–994 (2017).
18. Y. Gong, M. J. Wagner, J. Zhong Li, M. J. Schnitzer, *Nat. Commun.* **5**, 3674 (2014).
19. J. M. Kralj, D. R. Hochbaum, A. D. Douglass, A. E. Cohen, *Science* **333**, 345–348 (2011).
20. T. Wada *et al*., *J. Mol. Biol.* **411**, 986–998 (2011).
21. A. Keppler *et al*., *Nat. Biotechnol.* **21**, 86–89 (2003).
22. S. Chamberland *et al*., *eLife* **6**, e25690 (2017).
23. D. Brinks, A. J. Klein, A. E. Cohen, *Biophys. J.* **109**, 914–921 (2015).
24. C. A. Baker, Y. M. Elyada, A. Parra, M. M. L. Bolton, *eLife* **5**, e14193 (2016).
25. S. T. Lim, D. E. Antonucci, R. H. Scannevin, J. S. Trimmer, *Neuron* **25**, 385–397 (2000).
26. S. L. Smith, I. T. Smith, T. Branco, M. Häusser, *Nature* **503**, 115–120 (2013).
27. B. Tasic *et al*., *Nat. Neurosci.* **19**, 335–346 (2016).
28. M. B. Ahrens *et al*., *Nature* **485**, 471–477 (2012).
29. T. Hige, Y. Aso, G. M. Rubin, G. C. Turner, *Nature* **526**, 258–262 (2015).
30. A. Wang, J. Feng, Y. Li, P. Zou, *ACS Chem. Neurosci.* **9**, 639–650 (2018).

ACKNOWLEDGMENTS

We thank the Vivarium, Cell Culture, Instrument Design and Fabrication, Imaging, Molecular Biology, and Virus Production facilities at Janelia for assistance. Specifically, we thank B. Shields, D. Walpita, J. Cox, C. McGlynn, D. Alcor, A. Taylor, J. Rouchard, K. Ritola, X. Zhang, and J. Towne. We thank Z. Wei for discussions on data analysis. **Funding:** Supported by HHMI (A.S.A., T.K., A.S., O.N., H.L., Y.S., J.Y., J.Z., J.B.G., R.P., B.D.M., J.J.M., K.P., G.C.T., Z.L., M.K., K.S., M.B.A., L.D.L., and E.R.S.), Simons Collaboration on the Global Brain research awards 325171 and 542943SPI (M.B.A. and L.P.), IARPA MICRONS D16PC00003 (L.P.), NIH R01EB22913 (L.P.), Taiwan Ministry of Science and Technology MOST106-2628-B-010-004, MOST105-2628-B-010-005, MOST106-2320-B-010-012 and Taiwan National Health Research Institute NHRI-ex-107-10509NC (T.-W.C. and B.-J.L.), and the Allen Institute for Brain Science (L.C., S.C.S., and G.J.M.). **Author contributions:** A.S.A., L.D.L., and E.R.S. conceived the project. A.S.A. engineered Voltron. A.S.A., H.L., J.Z., J.B.G., R.P., J.J.M., Z.L., L.D.L., and E.R.S. performed and analyzed in vitro experiments. T.K., J.F., L.P., M.K., and M.B.A. performed and analyzed experiments in larval zebrafish. A.S., O.N., Y.-C.H., L.C., S.C.S., J.Y., G.J.M., K.P., B.-J.L., T.-W.C., and K.S. performed and analyzed mouse experiments. Y.S. and G.C.T. performed and analyzed experiments in *Drosophila*. L.P., J.J.M., G.J.M., K.P., B.-J.L., T.-W.C., G.C.T., Z.L., M.K., K.S., M.B.A., L.D.L., and E.R.S. supervised various aspects of this work. A.S.A. and E.R.S. wrote the manuscript with input and assistance from B.D.M. and all other authors. **Competing interests:** A.S.A., L.D.L., and E.R.S. have filed for a patent on chemigenetic voltage indicators. **Data and materials availability:** All data are available in the manuscript or the supplementary materials. Plasmids and AAVs are available from Addgene (www.addgene.org), transgenic *Drosophila* stocks are available from the Bloomington Drosophila Stock Center (https://bdsc.indiana.edu), and transgenic zebrafish are available from the Zebrafish International Resource Center (https://zebrafish.org/). J.B.G. and L.D.L. are inventors on U.S. Patents 9,933,417, 10,018,624, and 10,161,932 as well as U.S. Patent Application 16/211,388 held/submitted by HHMI; these cover azetidine-containing fluorophores such as JF$_{525}$. A.S.A., L.D.L., and E.R.S. are inventors on patent application WO2018102577A1 submitted by HHMI that covers chemigenetic voltage indicators. DNA plasmids and AAVs, transgenic zebrafish, and transgenic flies described in this manuscript are available from Addgene, ZIRC, and the Bloomington Drosophila Stock Center, respectively, under a material agreement with HHMI.

SUPPLEMENTARY MATERIALS

science.sciencemag.org/content/365/6454/699/suppl/DC1
Materials and Methods
Tables S1 to S5
Figs. S1 to S45
References (*31*–*62*)

5 October 2018; accepted 17 July 2019
Published online 1 August 2019
10.1126/science.aav6416